Inorganic Chemistry

Article

pubs.acs.org/IC

Computational Design of Two-Photon Fluorescent Probes for a Zinc Ion Based on a Salen Ligand

Shuang Huang,[†,‡] Lu-Yi Zou,[†] Ai-Min Ren,*[,†] Jing-Fu Guo,[§] Xiao-Ting Liu,[†] Ji-Kang Feng,[†] and Bao-Zhu Yang[‡]

[†]State Key Laboratory of Theoretical and Computational Chemistry, Institute of Theoretical Chemistry, Jilin University, Changchun 130023, People's Republic of China

[‡]School of Mathematics and Physics, Changzhou University, Changzhou 213164, People's Republic of China

[§]School of Physics, Northeast Normal University, Changchun 130021, People's Republic of China

Supporting Information

ABSTRACT: A two-photon fluorescent probe has become a critical tool in biology and medicine owing to its capability of imaging intact tissue for a long period of time, such as in two-photon fluorescence microscopy (TPM). In this context, a series of Salen-based zinc-ion bioimaging reagents that were designed based on an intramolecular charge-transfer mechanism were studied through the quantum-chemical method. The increase of one-photon absorption and fluorescence emission wavelength and the reduction of the oscillator strength upon coordination with a zinc ion reveal that they are fluorescent bioimaging reagents used for ratiometric detection. When the Salen ligand is incorporated with Zn^{2+}, the value of the two-photon absorption (TPA) cross-section (δ_{max}) will decrease, and most of the ligands and complexes exhibit a TPA peak in the near-infrared spectral region. That is, a substituent at the end of the ligand can influence the luminescence property, besides increasing solubility. In addition, the effect of an end-substituted position on the TPA property was considered, such as ortho and meta substitution. The detailed investigations will provide a theoretical basis to synthesize zinc-ion-responsive two-photon fluorescent bioimaging reagents as powerful tools for TPM and biological detection in vivo.

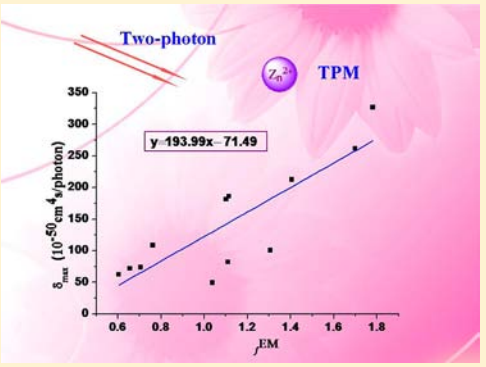

1. INTRODUCTION

In recent years, enormous interest in the design, synthesis, characterization, and photophysical investigation of fluorescent compounds with large two-photon absorption (TPA) cross sections has been increasing owing to their significant applications in a variety of areas, particularly in rapidly developing fields, such as multiphoton fluorescence imaging,[1] upconverted lasing,[2] optical data storage and switching,[3] optical sensor protection,[4] laser dyes,[5] three-dimensional microfabrication,[6] and photodynamic therapy.[7]

Compared with one-photon microscopy, two-photon fluorescence microscopy (TPM) with two lower-energy photons as the excitation source has become a popular tool for live-cell detection. It can be used in the fields of biology and medicine with the advantages of deeper penetration depth (>500 μm), lower tissue autofluorescence and self-absorption, intrinsically localized excitation, and reduction of photodamage and photobleaching.[8−10] Moreover, compared with UV−visible absorption spectra, the TPA wavelength located in the near-infrared (NIR) spectral region will be more suitable for biological detection and as a marker, which can completely eliminate the interference of background light.[11] Hence, the significant issue is to search efficient two-photon (TP) fluorescent probes with larger TPA cross sections in the NIR spectral region for clarifying various biological mechanisms in live tissues.

The investigation of a TP fluorescent probe acting as a new area has risen in recent years, which has attracted great interest of many chemical researchers. It shows stronger developmental potentials and broad application prospects. Also, more new researches are urgently needed. The current investigations of a TP fluorescent probe contain cation probe, anion probe, pH probe, and polar probe toward object identification; with regard to the identification mechanism for the probe, received identification mechanisms include photoinduced electron transfer (PET), intramolecular charge transfer (ICT), fluorescence resonance energy transfer, and excited-state proton transfer. The PET and ICT mechanisms are common and have been extensively investigated and successfully applied to live-cell imaging of a metal ion.[12−15] When a fluorophore is directly connected with a receptor and a π-conjugated system is formed with terminal electron-rich and -poor groups, ICT from electron donor to electron acceptor will enhance upon excitation by a strong light. When a metal-ion receptor plays the role of electron donor in the whole molecule, the electron-donating character of the metal-ion receptor will reduce, and a blue shift of the emission spectrum will accompany. However, if the metal-ion receptor

Received: October 10, 2012
Published: May 8, 2013

acts as an electron acceptor, the push−pull electron effect will further be strengthened by the interaction between the receptor and metal ion, and then the emission spectrum will show a red shift. This reveals that this type of molecule can serve as a fluorescent probe used for ratiometric detection and can be applied in different fields of measurement. Moreover, in the experiment, it is revealed that this series of fluorescent probes allows measurement of the fluorescence intensity at two wavelengths,[16,17] which may potentially reduce the influence on fluorescence signals, including the probe concentration, sample environment, and light scattering.[18,19] This technique provides greater precision measurement than that at a single wavelength, and it is suitable for the research on cellular imaging. Recently, more and more fluorescent probes have been successfully synthesized and applied for fluorescence detection and targeted molecular imaging in living cells.[20,21]

A variety of metal ions in vivo have special physiological functions and play crucial roles in the life course.[22] So, detection of the metal ion has become a hot issue. To understand the roles in cell biology, it is pivotal to detect the subcellular distribution in normal and abnormal cells with specific diseases using TPM. Zinc ion (Zn^{2+}) as the second most abundant transition metal in the human body has attracted a great deal of attention ascribing to the biological significance of Zn^{2+}, which plays an important role in biological processes, for instance, gene expression, apoptosis, brain function and pathology, and immune function.[23−27] Moreover, the Zn^{2+} complex exhibits low cytotoxicity to living cells and has better subcellular selectivity,[28−30] so it can penetrate into cells for in vivo detection. Therefore, it is significant to develop a Zn^{2+}-specific TP fluorescent probe. Of course, the selectivity and sensitivity of TP fluorescent probes for the zinc ion cannot be ignored, whose developments have received considerable attention in modern analytical chemistry, owing to their utilities in clarifying and analyzing the roles of ions and biomolecules in living system.[31−36] So, it is a critical challenge to explore excellent TP fluorescent probes for metal-ion detection in live cellular environments. A Zn^{2+}-specific TP fluorescent probe not only can be easily synthesized but also have improved sensitivity, selectivity, and stability, while all the above can be predicted by theoretical calculation first.

In 1987, the first zinc-ion fluorescent probe was discovered, which shows the change of conformation when zinc cytochrome fluorescence acts as a probe in cytochrome oxidase.[37] Also, then many types of Zn^{2+} fluorescent probes have been developed in succession; most of them can be applied to detecting Zn^{2+} in living cells,[38−42] which has made outstanding contributions to the exploration of the functions and properties and the binding mode for the zinc ion in organisms.[29,43−45] However, the theoretical research of Zn^{2+} fluorescent probes is limited; the primary reason is that the theory is immature and the cognition for the molecular probe is not perfect, so that the theoretical study on probe molecules is just in its infancy. At the present stage, theoretical investigations include geometry optimization, OPA spectrometry, or orbital energy calculations, but systematic reports on the TPA property do not arise, such as the change of the TPA cross section when the ligand binds to the metal ion.[46−48] In our quantum-chemical study, first of all, the accuracy of the computational method can be verified through calculation of the correlated data from the experiment. Second, the TPA property and detection principle can be studied systematically. Furthermore, the influence factors will be analyzed in detail. At last, the practical applications for the studied molecules will be explored legitimately. The systematic calculations will provide a useful theoretical basis for the experimental synthesis of the fluorescent probes with excellent TPA properties and supply theoretical guidance for the detection of zinc ion in living cells.

Recently, Hai et al. have synthesized a series of TP fluorescent bioimaging reagents based on the Salen ligand (L), which is named as the salicylaldehydoethylenediamine derivative and abbreviated as "Salen".[28] In particular, both ZnL_4 and ZnL_7 can be applied in TPM imaging in living cells to stain HeLa cells. These luminescent complexes show good chemo- and photostability, low cytotoxicity, and high subcellular selectivity, which are essential to become ideal TP fluorescent probes for live-cell detection. More importantly, the large values of TPA cross sections reveal that they are potentially used for TPM imaging.[28] In the present work, not only are the complexes selected for the theoretical investigation, but also their corresponding ligands are studied together. On the basis of the ligand-complex molecules, the ICT mechanism will be adopted to design novel zinc-ion bioimaging reagents. Besides the theoretically studies on OPA, TPA, and fluorescence properties, the binding energy, binding enthalpy, and Gibbs free energy of the reaction of TP fluorescent bioimaging reagents binding to the zinc ion will be discussed.

2. THEORETICAL METHODOLOGY

2.1. Choice of Functionals in the Computational Method. In order to choose suitable functionals to optimize the molecular geometries and calculate their optical properties in ground and excited states, complex ZnL_2 is taken as an example to be calculated with different functionals. Besides the common hybrid functional B3LYP (containing a 20% proportion of the Hartree−Fock exchange energy),[49−51] a long-range-corrected functional CAM-B3LYP (Coulomb-attenuating model)[52,53] was attempted, which contains just 19% exact exchange in the short range (like a conventional hybrid) and 65% in the long range. The MPWB1K functional was also tested because it can give the best performance for charge-transfer, hydrogen-bonding, and weak interactions.[54,55] Moreover, the M05-2X and M06-2X[56,57] functionals fitted for the transition metal were also tried. Herein, all of the functionals are implemented with a 6-31G(d,p) basis set.[58,59] The calculated OPA and emission wavelengths (λ^{O}_{max} and λ^{EM}_{max}) and corresponding oscillator strengths (f^{O} and f^{EM}) are shown in Table 1.

Table 1. OPA and Fluorescence Emission Spectra of ZnL_2 Calculated by Different Functionals in DMSO

	OPA		fluorescence emission		corrected
method	λ^{O}_{max}/nm[a]	f^{O}	λ^{EM}_{max}/nm	f^{EM}	λ^{EM}_{max}/nm[b]
B3LYP/6-31G**	565.8	0.8638	693.3	0.9765	666.9
	360.5	0.8453			
CAM-B3LYP/6-31G**	479.2	0.9964	618.6	1.0665	621.6
	336.9	0.6730			
MPWB1K/6-31G**	467.8	1.2187	559.9	1.4566	562.9
	308.3	0.662			
M05-2X/6-31G**	469.3	1.1561	601.5	1.1958	604.0
	337.2	0.6516	373.9	1.4962	
M06-2X/6-31G**	474.3	1.1857	613.6	1.2058	616.0
	341.7	0.689			

[a]The experimental OPA wavelengths of ZnL_2 are 593 and 385 nm (see ref 28). [b]The experimental fluorescence emission wavelength of ZnL_2 is 633 nm (see ref 28).

dx.doi.org/10.1021/ic3022062 | Inorg. Chem. 2013, 52, 5702−5713

The results show that OPA maxima calculated by the B3LYP functional are in reasonable agreement with the experimental values, while the emission maximum calculated by the CAM-B3LYP functional well approaches to the experimental data after solvent correction. Although the B3LYP functional has defects in dealing with the ICT system, it hs little influence on the OPA spectrum for the studied molecule. In all probability, the overestimation for the OPA wavelength has been offset by some other factors. However, during the emission process, the B3LYP functional often provides an improper description of the excited state with pronounced charge-transfer character, so the larger overestimation of the fluorescence emission wavelength (60 nm) calculated by the B3LYP functional must be resolved seriously. To some extent, it can be overcome by utilizing long-range-corrected functionals such as CAM-B3LYP, so that the B3LYP functional combined with the standard 6-31G(d,p) basis set was primarily adopted to optimize the molecular equilibrium geometries in the ground state and calculate the OPA spectra, while the CAM-B3LYP functional was applied to optimize the equilibrium geometries in the excited state and computation on fluorescence emission spectra. All of the above was carried out in the *Gaussian 09* program package (revisions A.02 and B.01).[60] In summary, the calculated results agree well with the experimental data for all of the synthesized molecules, which are shown in Table S1 (in the Supporting Information).

2.2. Solvent Correction. The OPA and fluorescence emission spectra were measured in a dimethyl sulfoxide (DMSO) solvent during the experiment, so the solvent effect included in the theoretical calculation is important to reproduce the experimental spectra with reasonable accuracy. To achieve the objective, the solvent effect was simulated using the polarizable continuum model (PCM) incorporated in the program of *Gaussian 09* during the present quantum-chemical computation. It is worth noting that the emission spectrum is deeply influenced by the solvent effect,[61,62] so further solvent correction must be carried out to modify emission spectra, which could be achieved by employing the state-specific correction method in *Gaussian 09* based on the equilibrium geometries in the excited state.

2.3. Calculation of the TPA Process. During the TPA process, the TPA efficiency can be characterized by the TPA cross section $[\delta(\omega)]$ at optical frequency $\omega/2\pi$, and it is directly related to the imaginary part of the third-order polarizability $[\gamma(-\omega;\omega,\omega,-\omega)]$,[63] as shown in eq 1

$$\delta(\omega) = \frac{3(\hbar\omega)^2}{2n^2c^2\varepsilon_0\hbar}L^4\mathrm{Im}[\gamma(-\omega;\ \omega,\ -\omega,\ \omega)] \tag{1}$$

where $\hbar\omega$ is the energy of the incoming photons, c is the speed of light, ε_0 is the vacuum electric permittivity, n indicates the refractive index of the medium, and L corresponds to the local-field factor, which is defined as $L = (n^2 + 2)/3$. During the present calculation, n is set as 1, so L is equal to 1 because of isolated molecules in the vacuum.

The perturbation theory is used to deduce the sum-overstates (SOS) expression applied to evaluating the components of the third-order polarizability ($\gamma_{\alpha\beta\gamma\delta}$). Considering a Taylor expansion of energy for the applied field, the Cartesian components of $\gamma_{\alpha\beta\gamma\delta}$ are given as refs 64 and 65.

To compare the calculated TPA cross section with the experimental one, the damping factor (Γ) of the excited state K in the SOS expression is set as 0.16 eV in our work. Also, the orientationally averaged (isotropic) value of γ is evaluated and defined as

$$\langle\gamma\rangle = \frac{1}{15}\sum_{i,j}(\gamma_{iijj} + \gamma_{ijij} + \gamma_{ijji}), \quad i,\ j = x,\ y,\ z \tag{2}$$

After $\langle\gamma\rangle$ is substituted into eq 1, the value of the TPA cross section is obtained.

Generally, the position and relative strength of the TP resonance are predicted using the following simplified form of the SOS expression:[66]

$$\delta \propto \frac{M_{0k}{}^2 M_{kn}{}^2}{(E_{0k} - E_{0n}/2)^2\Gamma} + \frac{M_{0n}{}^2\Delta\mu_{0n}{}^2}{(E_{0n}/2)^2\Gamma} \tag{3}$$

where M_{ij} is the transition dipole moment from the state i to j ($i, j = 0, k$, and n), E_{ij} is the corresponding excitation energy, the subscripts 0, k, and n refer to the ground state S_0, the intermediate state S_k, and the TPA final state S_n, respectively, and $\Delta\mu_{0n}$ is the difference of the dipole moment between S_0 and S_n.

In principle, any kind of self-consistent-field molecular orbital theory coordination with configuration interaction (CI) can be used to calculate the physical values according to the above expression. Then, the property of the electronic excited states was obtained by single- and double-electron excitation CI employing the *ZINDO* program.[67] It is well-known that the original *ZINDO* algorithm (obtained by Zerner) has only adopted single CI, while a double excitation configuration also needs to be considered for the correct determination of the third-order polarizability and TPA spectrometry. Thus, the double excitation configuration was added in the *ZINDO* calculation, which was compiled and proposed by our group and named as *FTRNLO*.[68,69] In this paper, the CI-active spaces were restricted to 20 highest occupied and 20 lowest unoccupied π orbitals in single CI and 4 highest occupied and 4 lowest unoccupied π orbitals in double CI. There are in all 573 configuration states in the CI calculation. Utilizing the *FTRNLO* program, the third-order polarizability (γ) and the TPA cross section (δ) were calculated according to eqs 1 and 2.

3. RESULTS AND DISCUSSION

3.1. Molecular Design and Geometry Optimization of the Ground State. A typical fluorescent probe molecule should contain a receptor (the recognition site) connected to a fluorophore (the signal source) that translates the recognition event into the fluorescence signal.[32] To achieve this objective, an ideal fluorescent probe molecule must meet two basic requirements; i.e., the receptor must have a stronger affinity to the relevant target (binding selectivity); on the basis of the good binding selectivity, the fluorescence signal should be able to avoid environmental interference (signal selectivity). Therefore, the design focuses on the search for a TP fluorophore that not only has a large TPA cross section and high fluorescence quantum yield but also whose emission wavelength lies in the NIR spectral region; moreover, the fluorophore should have better solubility. In order to obtain a larger TPA cross section, the TP fluorophore must have better π conjugation, a larger rigid plane, and a larger dipole moment of the excited state, but all of these will reduce the solubility.[70] The TP response depends on the strength of molecular polarization (the higher the polarization, the larger the value of the TPA cross section will be), so that a better TP effect will be obtained. It puts forward that the TPA cross section of a molecule ending with an amino group is approximately 10 times larger than that with alkoxy as the terminal group,[71] so the terminal group of a better TP fluorophore mostly consisted of an amine group. Moreover, it has been confirmed that a

dx.doi.org/10.1021/ic3022062 | *Inorg. Chem.* 2013, 52, 5702−5713

double-styrene-type fluorophore containing a cyano group (−CN) has a higher fluorescence quantum yield (>0.7).[72,73] Therefore, the ideal TP fluorophore should be a double-styrene derivative with two cyano groups and with amino as the terminal group.

Recently, a series of zinc-ion TP fluorescent bioimaging reagents based on the Salen ligand have been synthesized by Zhang and co-workers,[28] from which complexes ZnL_2, ZnL_3, ZnL_4, and ZnL_7 (with an electron donor as the terminal group) were selected for the theoretical investigations, together with their respective Salen ligands (L_2, L_3, L_4, and L_7). Also the change of the geometries and optical properties from a ligand (L) to metal complex (M-Salen) will be discussed in detail in the following sections. It is well-known that four atoms (O, N, N, and O) located in the center of Salen can ligands of some metal ions, forming M-Salen.[74] Generally, Salen occupies four coordination sites of metal in the plane, while the axial coordination is vacated. The diphenol H_2Salen is considered as the conjugated acid of the ligand that logically is $Salen^{2-}$. So as to discuss the change of the optical properties from the ligand to the corresponding Zn^{2+} complex, neutral ligands were adopted and called "Salen" ligands in this text because ZnL_n complexes are neutral.

Through analysis of the molecular structures of the reactant and product in the known reaction of probing Zn^{2+}, we reach a conclusion that TP fluorescent bioimaging of the Zn^{2+}-Salen complex can be explained by the ICT mechanism, because a strong ICT is formed between the amino group that acts as an electron-donor group at the end of the fluorophore and two cyano groups that act as electron acceptors at the top of the framework. It is worth mentioning that ICT will be of benefit to greatly increase the molecular TPA cross section. Thus, new ligands (L_{11} and L_{12}) with electron acceptors connecting to the N atoms, which are directly attached to the benzene ring, were designed. In addition, ligands L_{12}-OCH_3 and L_{12}-OCN were designed by means of replacing the N atoms with O atoms in the terminal groups (the structures are shown in Figure 1).

The two N and two O atoms in the molecular center (O, N, N, and O) can accept a zinc ion to form a four-coordination structure as Zn-Salen (shown in Figure 1), which can enhance the

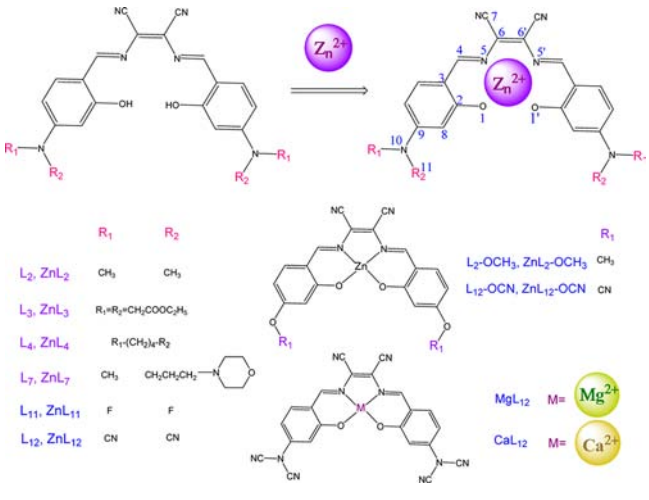

Figure 1. Structures of studied molecules.

molecular overall stability. In order to investigate the sensitivity of ligands for the zinc ion, ligand L_{12} was taken as an example to bind to the magnesium and calcium ions, respectively, forming complexes MgL_{12} and CaL_{12}.

The DFT//B3LYP/6-31G(d,p) method was adopted for optimizing molecular equilibrium geometries in the ground state. Then frequency calculation based on the optimized geometries was implemented; no imaginary frequency indicates that the equilibrium geometries are stable. Three views for each equilibrium geometry are presented in Figure 2. It shows that the central bodies of the studied molecules have C_2 symmetry. As is clearly seen from the elevation view, the two styrene branches turn close to the center as the ligand coordinates with Zn^{2+}, so the complexes become compact. As seen from the top and side views, the two styrene branches of the Zn^{2+} complex deviate more from the plane than those of the Salen ligand and lie on both sides of the plane, respectively, because Zn^{2+} commonly requires coordination with four ligands in tetrahedral geometry. Moreover, it is also influenced by the substituents at the end of the molecule. For example, the bulk of the terminal groups for ligands L_3 and L_7 are large, possessing greater steric hindrance, so that the substituents show serious deflection with two styrene branches off of the center plane (top and side views in Figure 2), exhibiting "tower-form" configurations. In addition, the C−C single bond (C3−C4, in Figure 1) between the benzene and C atom is not well fixed, resulting in its swing. However, the planarity of the designed molecules is better than that of the known ones.

Compared with ZnL_{12}, the stretching ability of the double-styrene branches for the MgL_{12} and CaL_{12} complexes is still strong, but the stretching direction of the two branches is different from that of ZnL_{12}, in which MgL_{12} and CaL_{12} stretch along with the body plane because of the requirement of both Mg^{2+} and Ca^{2+} for four ligands coordinated in square-planar geometry. That is, the double-styrene branches of the MgL_{12} and CaL_{12} complexes get away from the central C_2 axis, respectively, but they locate on the same plane, showing C_{2v} symmetry.

As listed in Table 2, the natural bond orbital (NBO) charge was analyzed; it reveals that with regard to all of the studied Salen ligands, the receptor part (CNCCNC + 2CN) located on the up side of the whole molecular skeleton acts as an electron acceptor, and the fluorophore distributed in the two branches plays the role of an electron donor. Therefore, ICT generates from the fluorophore to the receptor (CNCCNC + 2CN).

3.2. Thermodynamic Property. The binding energy (ΔE), binding enthalpy (ΔH), and Gibbs free energy (ΔG) of the binding reactions between the ligand and metal ions were calculated by the DFT method on the basis of equilibrium geometries and are shown in Table 3. It is worth noting that the basis set superposition error (BSSE) is very important.[75,76] The counterpoise (CP) method is one of the most usual methods to solve BSSE correction,[77] so the CP method is adopted to correct the BSSE of binding energies based on the B3LYP/6-31G(d,p) level.

It is well-known that the binding energy, binding enthalpy, and Gibbs free energy can evaluate the sensitivity and binding possibility of a probe molecule to a metal ion.[78−80] As is clearly seen from Table 3, the calculated results exhibit that the ΔE value of ligand L_{12} for Zn^{2+} is larger than that of Mg^{2+} and Ca^{2+}, so that ligand L_{12} is more sensitive to Zn^{2+}. The values of ΔH and ΔG for Zn^{2+} coordination reaction are much larger than those of Mg^{2+} and Ca^{2+}, respectively. This demonstrates that ligand L_{12} has a better binding possibility for the zinc ion.

3.3. One-Photon Absorption Property. The TD B3LYP/6-31G(d,p) method was implemented to calculate molecular OPA properties based on optimized geometries. The solvent effect (DMSO) was simulated using the PCM incorporated in the *Gaussian 09* program. As shown in Table S1 (in the Supporting Information),

dx.doi.org/10.1021/ic3022062 | *Inorg. Chem.* 2013, 52, 5702−5713

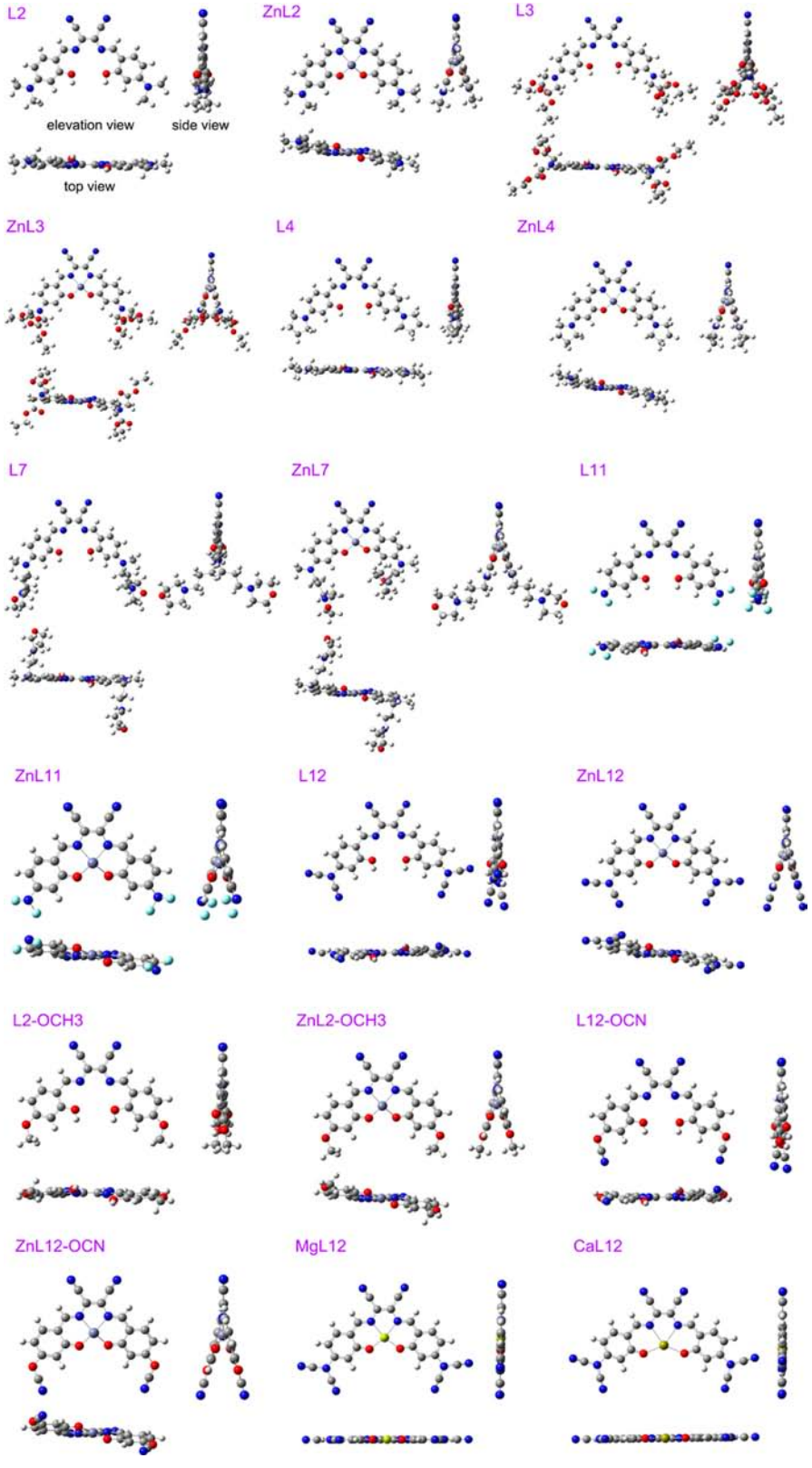

Figure 2. Optimized geometries of studied molecules.

the calculated results are in reasonable agreement with the experimental data, so it is feasible to analyze the OPA properties using the results. Besides, the *ZINDO* method was also adopted to calculate the OPA properties, and the results are summarized in Table S2 (in the Supporting Information); the good agreement between the calculated results and the experimental data can lay the foundation for the following calculation of the TPA properties.

The following are clearly seen from Table S1 (in the Supporting Information):

dx.doi.org/10.1021/ic3022062 | *Inorg. Chem.* 2013, 52, 5702−5713

Table 2. NBO Charge of the Receptor and Fluorophore in the Ground State for Studied Ligands

ligand	NBO charge	
	receptor (upside: CNCCNC + 2CN)	fluorophore (phenoxy group + substituent)
L_2	−0.2271	0.2271
L_3	−0.2094	0.2094
L_4	−0.2363	0.2363
L_7	−0.2261	0.2261
L_{11}	−0.1046	0.1046
L_{12}	−0.0987	0.0987
L_2-OCH_3	−0.3747	0.1791
L_{12}-OCN	−0.1085	0.1085

Table 3. Binding Energies (ΔE), Binding Enthalpies (ΔH), and Gibbs Free Energies (ΔG)

reaction	complex	ΔE (au)	ΔH (kJ/mol)	ΔG (kJ/mol)
$L_{12} + Zn^{2+} \rightarrow ZnL_{12}$	ZnL_{12}	−3320.13	−3319.87	−3319.97
$L_{12} + Mg^{2+} \rightarrow MgL_{12}$	MgL_{12}	−1741.19	−1740.90	−1740.99
$L_{12} + Ca^{2+} \rightarrow CaL_{12}$	CaL_{12}	−2218.66	−2218.36	−2218.46

(i) For complexes ZnL_2, ZnL_3, ZnI_4, and ZnL_7, their OPA maxima (λ^O_{max}) appear around 570 and 360 nm, respectively, and λ^O_{max} of their corresponding ligands (L) all locate at 540 and 330 nm. Obviously, λ^O_{max} shows a 30 nm (~975 cm^{-1} in the long-wavelength region and ~2525 cm^{-1} in the short-wavelength region) red shift upon Zn^{2+} binding, and the oscillator strength (f^O) in the long-wavelength region decreases and that in the short-wavelength region increases. Moreover, whether in the long- or short-wavelength region, λ^O_{max} values of L_4 and ZnL_4 are the longest and f^O values are the strongest among the studied ligands and complexes, respectively. It foreshows that a five-membered ring structure in the terminal group can play an important role on the OPA properties of Salen and Zn-Salen.

(ii) For the two molecules whose terminal group is replaced by an electron-withdrawing group (L_{11} and L_{12}), their λ^O_{max} values appear around 460 and 300 nm. Once ligands bind to Zn^{2+}, their λ^O_{max} values are present at 550, 400, and 330 nm, and the intensities of the three peaks are similar, but all are weaker than those of the corresponding ligands. Obviously, OPA wavelengths exhibit large red shifts as Zn-Salen ligands are formed.

(iii) When the N atom in the terminal group is replaced by an O atom (L_{12}-OCH_3 and L_{12}-OCN), λ^O_{max} values of the Zn-Salen ligands show red shifts at 60 and 84 nm (2312 and 3448 cm^{-1}) in the long-wavelength region and at 40 and 12 nm (3717 and 2563 cm^{-1}) in the short-wavelength region, respectively, while the values of f^O all decrease upon Zn^{2+} binding. Therefore, terminal substituents connected with O atoms can lead to larger red shifts upon coordination with Zn^{2+}.

(iv) As Zn^{2+} in the molecular center is replaced by Mg^{2+} or Ca^{2+} (MgL_{12} and CaL_{12}), the λ^O_{max} values of M-Salen ligands are both red-shifted compared with that of the ligand L_{12}, while f^O values decrease but are larger than that of ZnL_{12}. Both MgL_{12} and CaL_{12} have two OPA peaks, respectively, which is different from ZnL_{12}, which has three with similar intensity.

The transition in the long-wavelength region is composed of $S_0 \rightarrow S_1$ and characterized by H → L [H denotes the highest occupied molecular orbital (HOMO), and L denotes the lowest unoccupied molecular orbital (LUMO)], while that in the short-wavelength region is mostly H → L+1. However, for the complexes ZnL_{11}, ZnL_{12}, ZnL_{12}-OCN, MgL_{12}, and CaL_{12} with an electron acceptor as the terminal group, the transitions in the short-wavelength region are characterized by H−5 → L, H−4 → L, H−3 → L, or H−2 → L.

OPA maxima show red shifts as ligands coordinate with metal ions, and ΔE_{H-L} values of the corresponding molecules decrease as M-Salen ligands are formed (shown in Figure 3). This implies that the OPA process more easily takes place upon metal-ion binding.

3.4. Geometry Optimization of the Excited State and Fluorescence Property. To utilize the merits of range-separated and global hybrids, CAM was proposed as an applicable approach for calculation of the excited state, which has been validated in section 2.1. Thus, the CAM-B3LYP functional combined with the 6-31G(d,p) basis set was applied for geometry optimization in the first excited state (S_1, in DMSO solvent) on the basis of the equilibrium geometries obtained in the ground state (S_0). Herein, some molecules were taken as examples to investigate the change of optimized geometries in the bond length (B), bond angle (A), and dihedral angle (D) from S_0 to S_1. As mentioned above, the main skeletons of the studied molecules have C_2

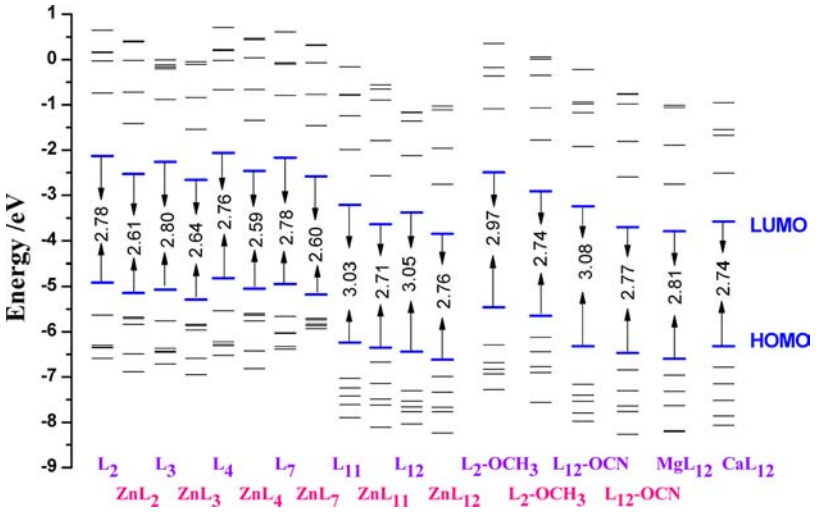

Figure 3. Predicted molecular orbital energy diagrams.

dx.doi.org/10.1021/ic3022062 | Inorg. Chem. 2013, 52, 5702−5713

symmetry, so B, A and D of the two branches are equal. Some representative values of one branch are listed in Tables S3 (in the Supporting Information) and 4.

As shown in Tables S3 (in the Supporting Information) and 4, the changes of B, A, and D from S_0 to S_1 are described as follows (atomic labeling is exhibited in Figure 1):

(i) Bond length (B): B2−3, B4−5, and B6−6′ get bigger; therefore, B6−6′ changes are much larger from 0.04 to 0.06 Å, indicating that the two branches tend to stretch, while B5−6, B6−7, B2−8, and B9−10 reduce. With regard to B3−4, the value of the free ligand decreases and that of the Zn^{2+} complex increases from S_0 to S_1, showing that the zinc ion strongly combines with the benzene ring and is near the central N atom in the first singlet excited state.

(ii) Bond angle (A): A1−2−3, A3−4−5, A2−1−Zn, and AZn−5−4 decrease; therefore, A2−1−Zn decreases 4−6°, and AZn−5−4 reduces around 2°, but the values of MgL_{12} change a little, while A2−3−4, A8−9−10, and A1−Zn−5 increase. This demonstrates that, in the configuration of the first singlet excited state, the two branches turn close to the center, and the whole molecule gets slender.

(iii) Dihedral angle (D): The decrease of D3−4−5−6 indicates that the planarity of molecular upside (CNCCNC + 2CN) gets better. With regard to the angle between the receptor and fluorophore, shown as D1−2−3−4, the free ligand increases and that of the Zn^{2+} complex decreases, indicating that the whole planarity gets better when the ligand binds to Zn^{2+}. However, the body skeletons of the geometries have more changes; in particular, the two branches of the ligand are seriously distorted. The D1−5−5′-1′ value generally displays the distortion of the two branches, in which L_{11} reaches 46°.

Different from ZnL_{12}, the increase of the bond lengths B1−Mg and B5−Mg for MgL_{12} shows that the two branches get away from the central metal ion. Moreover, the main skeleton of MgL_{12} has always maintained coplanarity, which exhibits C_{2v} symmetry. Also, the configuration of CaL_{12} is similar to that of MgL_{12}.

Fluorescence emission spectra were calculated (in DMSO solvent) on the basis of the equilibrium geometries in the first excited state. Then they were corrected through state-specific solvent correction. The calculated fluorescence emission maxima (λ^{EM}_{max}) and the corrected λ^{EM}_{max}, oscillator strength (f^O), and transition nature are shown in Table 5. It exhibits that the corrected λ^{EM}_{max} well agrees with the experimental data for all os the synthesized molecules.

As is clearly seen from Table 5, the range of fluorescence emission spectra is 550−630 nm, and it exhibits a red shift as the Salen ligand coordinates with Zn^{2+}. The oscillator strength decreases, which indicates that the fluorescence intensity reduces upon Zn^{2+} binding. For example, the red shift of 45 nm (1321 cm^{-1}) will occur when the ligand L_2-OCH_3 binds to Zn^{2+}, accompanying a decrease of the oscillator strength by half. So, this series of ligands can become fluorescent bioimaging reagents used for ratiometric detection, and ligand L_2-OCH_3 has the potential to be a better one, emitting yellow-orange light. However, for Mg^{2+} and Ca^{2+}, once they integrate with L_{12}, fluorescence emission spectra exhibit 53 nm (1618 cm^{-1}) and 33 nm (976 cm^{-1}) blue shifts, respectively, and the oscillator strengths increase. This reflects the difference between ligand L_{12} binding to Zn^{2+} and coordinating with other metal ions (Mg^{2+} and Ca^{2+}), implying that the ability of L_{12} identifies a zinc ion.

To distinctly present the relationship between the fluorescence intensity (f^{EM}) and OPA intensity (f^O), the dependence

Table 4. Dihedral Angles (D) of Some Molecules in S_0 and S_1 (the Values in S_1 Are Shown in Parentheses)

D	L_4	ZnL_4	L_{11}	ZnL_{11}	L_2-OCH_3	ZnL_2-OCH_3	MgL_{12}
D1−2−3−4	0.07 (−0.17)	−3.45 (1.20)	−0.13 (−1.58)	−4.56 (2.249)	−0.22 (084)	−4.040 (1.80)	0.00 (0.00)
D3−4−5−6	−177.90 (−177.57)	−168.03 (−167.23)	178.16 (162.60)	−169.37 (−167.52)	−177.96 (−174.58)	−168.93 (−167.23)	0.00 (0.00)
D5−6−6′−5′	3.19 (1.80)	2.28 (−1.78)	−2.98 (−5.61)	2.51 (−2.88)	3.09 (2.02)	2.25 (−2.85)	0.00 (0.00)
D1−5−5′−1′	17.86 (8.41)	28.83 (37.19)	−20.71 (−66.26)	26.30 (37.22)	18.92 (21.43)	26.69 (37.42)	0.00 (0.00)
D8−9−10−11	−4.88 (−4.27)	−4.16 (−4.59)	−37.88 (−35.58)	−30.98 (−31.47)	0.07 (−0.06)	0.33 (−0.58)	0.00 (0.00)

dx.doi.org/10.1021/ic3022062 | Inorg. Chem. 2013, 52, 5702−5713

Table 5. Fluorescence Emission Spectra of Studied Molecules

molecule	λ^{EM}_{max}/nm	f^{EM}	corrected λ^{EM}_{max}/nm[a]	transition nature		
L_2	596.0	1.7289	600.1	S_0–S_1	H → L	0.69
					H−1 → L+1	0.10
ZnL_2	618.7	1.0665	621.5 (633)[a]	S_0–S_1	H → L	0.68
L_3	580.6	1.7280	584.2	S_0–S_1	H → L	0.69
					H−1 → L+1	0.10
ZnL_3	613.9	0.9750	616.8 (618)[a]	S_0–S_1	H → L	0.69
					H−2 → L+1	0.10
L_4	601.1	1.7815	605.3	S_0–S_1	H → L	0.69
					H−1 → L+1	0.10
ZnL_4	620.6	1.1138	623.5 (633)[a]	S_0–S_1	H → L	−0.68
L_7	598.4	1.6989	602.5	S_0–S_1	H → L	−0.69
					H−1 → L+1	−0.10
ZnL_7	614.1	1.1016	616.9 (635)[a]	S_0–S_1	H → L	0.68
L_{11}	604.2	0.9563	605.5	S_0–S_1	H → L	0.69
ZnL_{11}	610.1	0.6033	614.2	S_0–S_1	H → L	−0.69
					H−1 → L+1	0.10
L_{12}	597.2	1.0377	598.2	S_0–S_1	H → L	0.69
ZnL_{12}	601.7	0.7050	605.2	S_0–S_1	H → L	−0.69
L_2-OCH_3	559.3	1.4048	561.5	S_0–S_1	H → L	0.70
ZnL_2-OCH_3	603.0	0.7616	606.5	S_0–S_1	H → L	0.69
L_{12}-OCN	595.0	0.9473	596.1	S_0–S_1	H → L	0.69
ZnL_{12}-OCN	596.3	0.6553	599.9	S_0–S_1	H → L	0.69
MgL_{12}	543.0	1.1087	545.4	S_0–S_1	H → L	0.69
					H−1 → L+1	−0.12
CaL_{12}	562.5	1.3060	565.2	S_0–S_1	H → L	−0.69
					H−1 → L+1	−0.12

[a]The experimental fluorescence emission wavelengths are shown in parentheses and are from ref 28.

relationship between them is expressed in Figure 4. It shows that f^{EM} will enhance as f^{O} increases. That is to say, enhancement of

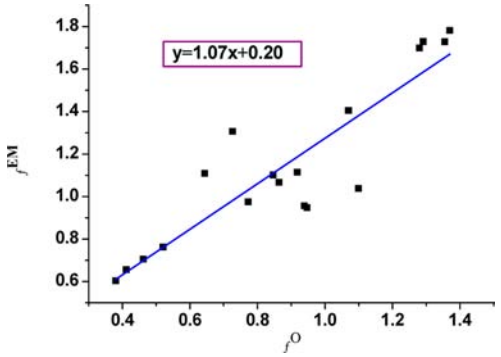

Figure 4. Relationship between f^{EM} and f^{O}.

the OPA intensity will result in a gradual increase of the fluorescence intensity with an approximate linear relationship described by $y = 1.07x + 0.20$.

It is well-known that a large Stokes shift can avoid interference of the absorption and emission spectra, which is critical to improving the sensitivity and accuracy of the testing. To achieve this objective, the Stokes shift of the studied ligands and metal complexes was analyzed, and its dependence on the OPA wavelength (λ^{O}) is depicted in Figure 5. It shows that most of the points evenly distribute on both sides of the line, except two deviated points composed of MgL_{12} and CaL_{12}. The deviation may be caused by the larger excited energy of MgL_{12} and CaL_{12}. Moreover, it exhibits that ligands L_{11}, L_{12}, and L_{12}-OCN whose

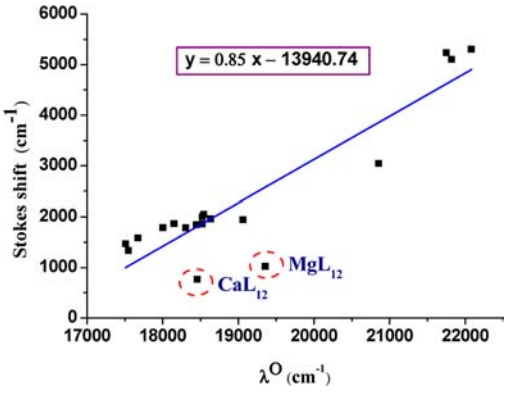

Figure 5. Dependence of the Stokes shift on λ^{O}.

N atoms in the molecular extremity are connected with an electron acceptor have a larger Stokes shift (140–145 nm; 5103–5304 cm^{-1}) than that of other ligands and metal complexes (20–80 nm; 764–3046 cm^{-1}). It confirms the superiority of the designed probes, whose terminal group is an electron acceptor.

The electron transition of all of the studied molecules is excited from S_0 to S_1, which is mainly assigned as the H → L transition, as shown in Table 5.

It is reported that the dipole moment (μ) will change upon binding to a metal ion with regard to the probe that originates from the ICT mechanism.[32,81] As is clearly seen from Table 6,

Table 6. Dipole Moments (μ_0 and μ_1) in the Ground and First Excited States (Unit: Debye)

molecule	μ_0	μ_1	molecule	μ_0	μ_1
L_2	15.3	22.2	ZnL_2	10.1	13.1
L_3	15.5	21.6	ZnL_3	10.9	14.0
L_4	16.1	23.2	ZnL_4	11.0	14.2
L_7	15.4	19.4	ZnL_7	10.0	13.0
L_{11}	6.0	9.3	ZnL_{11}	0.4	1.2
L_{12}	3.0	5.7	ZnL_{12}	3.8	5.1
L_2-OCH_3	13.8	19.4	Zn L_2.OCH_3	7.7	9.1
L_{12}-OCN	1.8	5.0	ZnL_{12}-OCN	4.5	6.0
MgL_{12}	3.8	5.0	CaL_{12}	1.4	0.3

μ_0 [dipole moment of the ground state (S_0)] and μ_1 [dipole moment of the first singlet excited state (S_1)] values for all of the studied molecules increase from S_0 to S_1, and the increased degree of ligands is larger than that of metal complexes, indicating that larger ICT occurs in the transition processes for each ligand. For molecules in which the N atoms in the terminal group are connected with an electron donor, the values of μ_0 and μ_1 are much larger than those of the molecules whose terminal N atoms are attached with an electron acceptor, respectively, while μ_0 and μ_1 values of MgL_{12} and CaL_{12} are both smaller than that of ZnL_{12}. In addition, except L_{12}-OCN, the values of μ_0 and μ_1 all reduce from ligands to the corresponding Zn^{2+} complexes, which will result in a reduction of the fluorescence intensity as Zn-Salen ligands are formed. In a word, the reduced polarization in the first excited state of the Zn-bound form is responsible for the weak fluorescence intensity and strong red shift of the fluorescence emission spectrum compared with that of an unbound free fluorophore ligand.

3.5. TPA Property. Usually, it is required that the TP excited wavelength of a TP fluorescent probe located in the NIR spectral region (650–900 nm) is taken into account for practical

dx.doi.org/10.1021/ic3022062 | Inorg. Chem. 2013, 52, 5702–5713

application in a biological system.[82,83] So, the TPA properties for the studied molecules in the wavelength range of 490−1000 nm were calculated by applying the *ZINDO* program in DMSO solvent. Also, 300 states were chosen, which is ascertained to be sufficient for convergence of the TPA cross section (δ_{max}), taking the largest molecule ZnL_7 as an example. The relationship between the calculated δ_{max} and the number of excited states is shown in Figure 6, which suggests that δ_{max} values come to

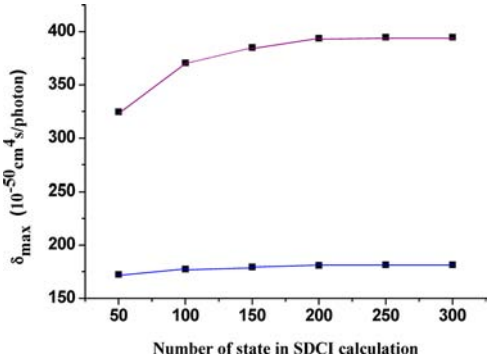

Figure 6. Dependence of the TPA cross section (δ_{max}) on the number of excited states for ZnL_7.

convergence when the number of excited states is 300, revealing that it is sufficient for describing the electronic structures of low-lying excited TPA target states. Thus, 300 excited states were applied to the calculation on all of the studied molecules. The calculated results are displayed in Tables 7 and S2 (in the Supporting Information).

It can been clearly seen that all of the studied molecules exhibit strong TPA maxima (λ^T_{max}) between 502.0 and 892.0 nm; moreover, each molecule has more than one peak except L_{11}. On the one hand, most of ligands and complexes have large values of δ_{max} in the wavelength range of 676.0−834.4 nm, which locates in the NIR spectral region, except L_{11} and L_{12}-OCN. Also, the value of δ_{max} decreases 80−150 GM as the ligand is incorporated with the zinc ion, except that δ_{max} values for L_3 and L_{12} get larger upon zinc-ion binding. On the other hand, all of the ligands have much larger δ_{max} (1071.7−2652.2 GM) in the wavelength range of 498.3−612.0 nm, and the value of δ_{max} reduces 334−2321 GM as the ligand combines with Zn^{2+}. The reason is that the skeleton of the Zn^{2+} complex becomes distorted as the free ligand coordinates with the zinc ion. That is, compared with Zn^{2+} complexes, the main skeletons of the free ligands have better planarity, which benefits ICT, so they have larger values of δ_{max}. Thus, most of the studied ligands can become TP fluorescent bioimaging reagents applied for Zn^{2+} detection in vivo. In a word, reasonably changing the terminal group can enhance TP fluorescence responsiveness for the zinc ion, and it is feasible to achieve ideal TP fluorescent bioimaging reagents in this way.

However, if Zn^{2+} in the molecular center is replaced by Mg^{2+} or Ca^{2+}, TPA peaks of the complexes MgL_{12} and CaL_{12} show blue shifts compared with ZnL_{12}. Also, the values of δ_{max} for CaL_{12} and MgL_{12} are larger than that of ZnL_{12}, implying that ligand L_{12} shows different phenomena to identify Zn^{2+} from Ca^{2+} and Mg^{2+}.

In addition, the position of the terminal group was considered, such as ortho and meta substitution. Herein, ligand L_4 and complex ZnL_4 were taken as examples (L_4-O, L_4-M, ZnL_4-O, and ZnL_4-M), and the correlated calculated results are presented in Table S2 (in the Supporting Information). It shows that the values of δ_{max} for ortho- and meta-substituted ligands and Zn^{2+} complexes are smaller than those of the corresponding para-substituted molecules in the long-wavelength region. Because larger steric hindrance will generate when terminal groups and double-styrene branches locate at the ortho or meta position, this will lead to serious distortion of the molecular structures, so that molecular planarity will reduce, eventually resulting in smaller values of δ_{max}. Therefore, the position of end substitution cannot be ignored. Little steric effect will be generated via para substitution; that is, when the styrene and terminal groups locate at the relative position, as shown in Figure 1, better planarity will be obtained, so that larger value of δ_{max} will be achieved.

Because binding of the electropositive metal ion will cause a decrease of the electron donor capacity, the value of the TPA cross section will be lowered inevitably and the brightness of the fluorescence emission will be reduced. What is the relationship between the TPA cross section and fluorescence intensity? The description of Figure 7 clearly shows an approximate proportional relationship as $y = 193.99x - 71.49$, which has validated the conclusion in the experiment that the fluorophore brightness is proportional to the TPA cross section and fluorescence quantum yield.[84] However, up to now, the theoretical calculation on the fluorescence quantum yield cannot be implemented because of the complexity and intractability for the nonradiative transition process, so the relationship between the fluorescence brightness and fluorescence quantum yield cannot be simulated in theory currently.

To distinctly present the influence on the changing nature of the TPA properties for the studied molecules, a three-state approximation was adopted for an explanation of the calculation results. In the SOS model, the three-state expression

$$X = \frac{M_{0k}^2 M_{kn}^2}{(E_{0k} - E_{0n}/2)^2 \Gamma} + \frac{M_{0n}^2 \Delta\mu_{0n}^2}{(E_{0n}/2)^2 \Gamma}$$

was introduced by only considering three important states (the ground, charge-transfer, and TPA final states). The approximate proportional relationship between δ_{max} and X during the TPA process (depicted in Figure 8) implies that X can predict the changing tendency of δ_{max} in general, according to the formulation $y = 0.01x - 73.79$. As seen from the parameters described in Table S4 (in the Supporting Information), the transition dipole moments (M_{0k}, M_{kn}, and M_{0n}) of the ligands are larger than those of metal complexes, respectively, and their values are larger than those of other factors, so transition dipole moments are critical factors influencing the value of δ_{max}. Although the transition energies (E_{0k} and E_{0n}) of all of the studied molecules are smaller, about 3−4 eV, they can also affect the values of δ_{max} to some extent. Simultaneously, the values of the difference for dipole moments between the ground and final states [$\Delta\mu_{0n} = \mu_n - \mu_0$; μ_0, $\mu_n = (\mu_x + \mu_y + \mu_z)^{1/2}$] for most ligands are larger than that of corresponding metal complexes, which can also result in a larger value of δ_{max} for the ligand compared with the corresponding M-Salen ligand, while the fact that the value of $\Delta\mu_{0n}$ for L_3 is smaller than that of ZnL_3 may be the reason why the δ_{max} value gets larger upon Zn^{2+} binding. In a word, the factors in the three-state expression X all play important roles on the TPA cross section.

3.6. Electronic Structure and ICT. As mentioned above, our studied molecules originate from the ICT mechanism, so charge transfer between an electron donor and an electron acceptor is an important factor that affects the change of the TPA cross section. In order to further interpret the internal factors influencing the TPA properties and to analyze the transition

dx.doi.org/10.1021/ic3022062 | *Inorg. Chem.* 2013, 52, 5702−5713

Table 7. OPA and TPA Properties of the Studied Molecules Calculated by the *ZINDO* Method

molecule	λ^{O}_{max}/nm[a]	f^{O}	λ^{T}_{max}/nm[a]	δ_{max}/GM[a]	transition nature		
L_2	511.8	0.9733	824.4	334.4	$S_0 \rightarrow S_1 \rightarrow S_2$	H−1 → L	−0.60
						H−3 → L	−0.40
	381.4	0.2634	612.0	1071.7	$S_0 \rightarrow S_6 \rightarrow S_{16}$	H−1 → L+1	−0.59
						H−4 → L+2	−0.33
L_2	511.8	0.9733	824.4	334.4	$S_0 \rightarrow S_1 \rightarrow S_2$	H−1 → L	−0.60
						H−3 → L	−0.40
	381.4	0.2634	612.0	1071.7	$S_0 \rightarrow S_6 \rightarrow S_{16}$	H−1 → L+1	−0.59
						H−4 → L+2	−0.33
ZnL_2	575.3 (593)[a]	0.4466	802.0	183.3	$S_0 \rightarrow S_1 \rightarrow S_5$	H−3 → L	−0.59
						H−1 → L	0.55
	401.5 (385)[a]	0.4917	685.0	392.7	$S_0 \rightarrow S_5 \rightarrow S_{12}$	H−4 → L	0.54
						H−3 → L+1	0.34
L_3	445.6	0.9045	696.5	201.4	$S_0 \rightarrow S_1 \rightarrow S_5$	H−1 → L	−0.64
						H → L+1	0.53
	348.2	0.5267	514.5	2652.2	$S_0 \rightarrow S_5 \rightarrow S_{24}$	H−2 → L+1	0.47
						H → L+3	0.45
						H,H → L,L	−0.35
ZnL_3	566.0 (578)[a]	0.4129	827.7	112.7	$S_0 \rightarrow S_1 \rightarrow S_4$	H → L+1	−0.67
						H−1 → L	0.46
						H, H → L, L	−0.33
	380.8 (378)[a]	0.4363	676.0	335.6	$S_0 \rightarrow S_5 \rightarrow S_{17}$	H−4 → L	0.46
						H−3 → L+1	0.40
						H → L+2	−0.36
L_4	505.4	0.9958	814.6	326.8	$S_0 \rightarrow S_1 \rightarrow S_5$	H−1 → L	0.69
	381.8	0.3096	608.4	1205.6	$S_0 \rightarrow S_6 \rightarrow S_{18}$	H, H → L+1, L+1	0.44
						H, H → L, L	0.34
						H−1 → L+2	0.34
ZnL_4	573.9 (593)[a]	0.4618	805.1 (840)[a]	186.0 (196)[a]	$S_0 \rightarrow S_1 \rightarrow S_5$	H−1 → L	0.62
						H−3 → L	−0.52
	402.6 (387)[a]	0.4869	682.7 (810)[a] (770)[a]	423.3 (161)[a] (96)[a]	$S_0 \rightarrow S_5 \rightarrow S_{13}$	H, H → L + 1, L + 1	−0.38
						H → L+2	0.33
L_7	486.0	0.9907	783.7	261.9	$S_0 \rightarrow S_1 \rightarrow S_4$	H−1 → L	0.71
						H → L+1	0.35
						H, H → L, L	0.33
	374.0	0.4773	576.1	1248.6	$S_0 \rightarrow S_6 \rightarrow S_{21}$	H−2 → L+1	−0.35
						H → L+8	−0.35
ZnL_7	570.7 (595)[a]	0.4485	786.7 (840)[a]	181.5 (181)[a]	$S_0 \rightarrow S_1 \rightarrow S_5$	H−1 → L	0.58
						H−3 → L	−0.55
	397.6 (387)[a]	0.4880	676.0 (810)[a]	394.7 (151)[a]	$S_0 \rightarrow S_5 \rightarrow S_{12}$	H−4 → L	0.49
						H−3 → L+1	0.39

[a]The experimental OPA and TPA wavelengths and cross sections are shown in parentheses and are from ref 28.

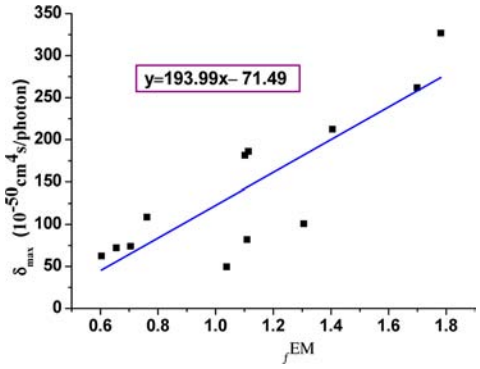

Figure 7. Relationship between the TPA cross section and fluorescence intensity.

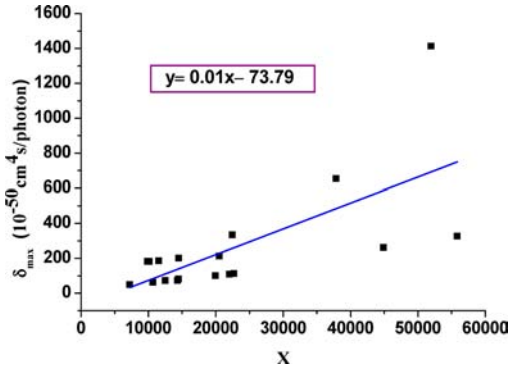

Figure 8. Relationship between δ_{max} and X of the studied molecules.

nature about the important excitations, a contour plot of molecular frontier orbitals of the ligands and their corresponding metal complexes related to the OPA and TPA processes was investigated and is presented in Figure S1 (in the Supporting Information). It shows that the electron clouds of the HOMO

dx.doi.org/10.1021/ic3022062 | Inorg. Chem. 2013, 52, 5702−5713

locate on the bonding π orbitals and those of the LUMO on unbonding π^* orbitals for the studied molecules, so the H → L transition is assigned as $\pi-\pi^*$ character.

Table S5 (in the Supporting Information) shows the net charge change ($\Delta Q = Q_n - Q_0$) of some parts for the studied molecules. Combined with Figure S1 in the Supporting Information, the ICT process was analyzed as follows. As seen from the H−2 → L+1 transition of L_7 and H−4 → L of ZnL_7, the electron cloud transfers from the terminal group to the upside of the ligand, illustrating the emergence of ICT from electron donor to electron acceptor. Also, abundant charge transfer appears from the two branches to the zinc ion in the molecular center with regard to the H−1 → L+7 transition of ZnL_2-OCH_3. Moreover, ΔQ values of Zn^{2+} for all of the complexes reveal that the zinc ion acts as an electron acceptor, despite less distribution of the electron cloud on Zn^{2+}. The sign of ΔQ illustrates that the receptor (CNCCNC + 2CN) of each molecule plays the role of electron acceptor, and the fluorophore (including the phenoxy group and terminal substituent) acts as an electron donor, showing that ICT occurs from the fluorophore to receptor. However, the values of ΔQ for the ligands L_{12} and L_{12}-OCN whose terminal group is an electron acceptor indicate that charge transfers from the phenoxy group to the receptor, which can be distinctly expressed via the change of electron clouds shown in Figure S1 in the Supporting Information.

4. SUMMARY

In summary, in DMSO solvent, the OPA, TPA, and fluorescence properties of a series of zinc-ion fluorescent bioimaging reagents on the basis of the Salen ligand designed by the ICT mechanism were investigated in theory. The studies indicate that both OPA and fluorescence emission spectra red shift at 4−90 nm (106−3600 cm^{-1}) after binding to Zn^{2+}, revealing that this series of ligands can become fluorescent bioimaging reagents used for ratiometric detection, and ligand L_2-OCH_3 has the potential to be a better one, emitting yellow-orange light. Moreover, the larger values of ΔE, ΔH, and ΔG for ZnL_{12} than that of MgL_{12} and CaL_{12} demonstrate that ligand L_{12} has a better binding possibility and sensitivity toward the zinc ion separated from Mg^{2+} and Ca^{2+}. During the TPA process, the TPA peaks for most of molecules locate in the NIR spectral region, 676.0−834.4 nm. Also, the values of δ_{max} decrease 80−150 GM when ligands coordinate with the zinc ion, except that L_3 and L_{12} get larger upon Zn^{2+} binding. So, reasonably changing the terminal group of the Salen ligand can obtain ideal TP fluorescent reagents for TPM. In a word, this series of Salen derivatives can serve as TP fluorescent bioimaging reagents for Zn^{2+} ratiometric detection in vivo.

■ ASSOCIATED CONTENT

Ⓢ Supporting Information

OPA properties of the studied molecules calculated by the time-dependent DFT method, OPA and TPA properties of the studied molecules calculated by the ZINDO method, bond lengths and angles of some molecules in S_0 and S_1 (the values in S_1 are shown in parentheses), factors of influence on maximum absorptions for studied molecules, net charge change of some parts for the studied molecules, contour surfaces of the frontier orbitals relevant to OPA and TPA processes, and Cartesian coordinates of the optimized geometries in the ground and first excited states. This material is available free of charge via the Internet at http://pubs.acs.org.

■ AUTHOR INFORMATION

Corresponding Author

*E-mail: aimin_ren@yahoo.com.

Notes

The authors declare no competing financial interest.

■ ACKNOWLEDGMENTS

This work is supported by the Natural Science Foundation of China (Grants 21173099 and 20973078), the Major State Basis Research Development Program (Grant 2013CB 834801), Natural Science Foundation of Jiangsu Provincial Department of Education (Grant SCZ1212400003), special funding to basic scientific research projects for Central Colleges, the Priority Academic Program Development of Jiangsu Higher Education Institutions, and the Foundation of State Key Laboratory of Theoretical and Computational Chemistry, Jilin University.

■ REFERENCES

(1) Bhawalkar, J. D.; He, G. S.; Prasad, P. N. *Rep. Prog. Phys.* **1996**, *59*, 1041.
(2) Lin, T. C.; Chung, S. J.; Kim, K. S.; Wang, X.; He, G. S.; Swiatkiewicz, J.; Pudavar, H. E.; Prasad, P. N. *Adv. Polym. Sci.* **2003**, *161*, 157.
(3) Reinhardt, B. A.; Brott, L. L.; Clarson, S. J.; Dillard, A. G.; Bhatt, J. C.; Kannan, R.; Yuan, L.; He, G. S.; Prasad, P. N. *Chem. Mater.* **1998**, *10*, 1863.
(4) Wu, L. Z.; Tang, X. J.; Jiang, M. H.; Tung, C. H. *Chem. Phys. Lett.* **1999**, *315*, 379.
(5) Fakis, M.; Polyzos, J.; Tsigaridas, G.; Parthenios, J.; Fragos, A.; Giannetas, V.; Persephonis, P.; Mikroyannidis, J. *Chem. Phys. Lett.* **2000**, *323*, 111.
(6) Wang, H. Z.; Lei, H.; Wei, Z. C.; Zhao, F. L.; Zheng, X. G.; Hu, N. S.; Wang, X. M.; Ren, Y.; Tian, Y. P.; Fang, Q.; Jiang, M. H. *Chem. Phys. Lett.* **2000**, *324*, 349.
(7) Ehrlich, J. E.; Wu, X. L.; Lee, L. Y. S.; Hu, Z. Y.; Rockel, H.; Marder, S. R.; Perry, J. W. *Opt. Lett.* **1997**, *22*, 1843.
(8) Zipfel, W. R.; Williams, R. M.; Webb, W. W. *Nat. Biotechnol.* **2003**, *21*, 1369.
(9) Helmchen, F.; Denk, W. *Nat. Methods* **2005**, *2*, 932.
(10) Williams, R. M.; Zipfel, W. R.; Webb, W. W. *Curr. Opin. Chem. Biol.* **2001**, *5*, 603.
(11) Greer, L. F.; Szalay, A. A. *Luminescence* **2002**, *17*, 43.
(12) Xu, Z.; Kim, G. H.; Han, S. J.; Jou, M. J.; Lee, C.; Shin, I.; Yoon, J. *Tetrahedron* **2009**, *65*, 2307.
(13) Xu, Z. C.; Baek, K. H.; Kim, H. N.; Cui, J. N.; Qian, X. H.; Spring, D. R.; Shin, I.; Yoon, J. *J. Am. Chem. Soc.* **2010**, *132*, 601.
(14) Zhang, X.; Hayes, D.; Smith, S. J.; Friedle, S.; Lippard, S. J. *J. Am. Chem. Soc.* **2008**, *130*, 15788.
(15) Qian, F.; Zhang, C.; Zhang, Y.; He, W.; Gao, X.; Hu, P.; Guo, Z. *J. Am. Chem. Soc.* **2009**, *131*, 1460.
(16) Li, D. H.; Shen, J. S.; Chen, N.; Ruan, Y. B.; Jiang, Y. B. *Chem. Commun.* **2011**, *47*, 5900.
(17) Coskun, A.; Akkaya, E. U. *J. Am. Chem. Soc.* **2005**, *127*, 10464.
(18) Xiang, Y.; Tong, A. *Luminescence* **2008**, *23*, 28.
(19) Li, N.; Tang, W. X.; Xiang, Y.; Tong, A. J.; Jin, P. Y.; Ju, Y. *Luminescence* **2010**, *25*, 445.
(20) Xue, L.; Liu, C.; Jiang, H. *Chem. Commun.* **2009**, 1061.
(21) Tomat, E.; Nolan, E.; Jaworski, J.; Lippard, S. *J. Am. Chem. Soc.* **2008**, *130*, 15776.
(22) Alberts, B.; Johnson, A.; Lewis, J.; Raff, M.; Roberts, K.; Walter, P. *Molecular Biology of the Cell*, 4th ed.; Taylor & Francis Group: New York, 2002.
(23) Falchuk, K. H. *Mol. Cell. Biochem.* **1998**, *188*, 41.
(24) Maret, W.; Jacob, C.; Vallee, B. L.; Fischer, E. H. *Proc. Natl. Acad. Sci. U.S.A.* **1999**, *96*, 1936.
(25) Cuajungco, M. P.; Lees, G. J. *Neurobiol. Dis.* **1997**, *4*, 137.
(26) Choi, D. W.; Koh, J. Y. *Annu. Rev. Neurosci.* **1998**, *21*, 347.

(27) Frederickson, C. J.; Koh, J. Y.; Bush, A. I. *Nat. Rev. Neurosci.* **2005**, *6*, 449.
(28) Hai, Y.; Chen, J. J.; Zhao, P.; Lv, H. B.; Yu, Y.; Xu, P. Y.; Zhang, J. L. *Chem. Commun.* **2011**, *47*, 2435.
(29) Manandhar, E.; Broome, J. H.; Myrick, J.; Lagrone, W.; Cragg, P. J.; Wallace, K. J. *Chem. Commun.* **2011**, *47*, 8796.
(30) Baek, N. Y.; Heo, C. H.; Lim, C. S.; Masanta, G.; Cho, B. R.; Kim, H. M. *Chem. Commun.* **2012**, *48*, 4546.
(31) Czarnik, A. W. *Acc. Chem. Res.* **1994**, *27*, 302.
(32) Silva, A. P. D.; Gunaratne, H. Q. N.; Gunnlaugsson, T.; Huxley, A. J. M.; McCoy, C. P.; Rademacher, J. T.; Rice, T. E. *Chem. Rev.* **1997**, *97*, 1515.
(33) Xu, Z.; Chen, X.; Kim, H. N.; Yoon, J. *Chem. Soc. Rev.* **2010**, *39*, 127.
(34) Beer, P. D.; Bayly, S. R. *Top. Curr. Chem.* **2005**, *255*, 125.
(35) Kim, S. K.; Lee, D. H.; Hong, J. I.; Yoon, J. *Acc. Chem. Res.* **2009**, *42*, 23.
(36) Caltagirone, C.; Gale, P. A. *Chem. Soc. Rev.* **2009**, *38*, 520.
(37) Alleyne, T. A.; Wilson, M. T. *Biochem. J.* **1987**, *247*, 475.
(38) Ahn, H. C.; Yang, S. K.; Kim, H. M.; Li, S. J.; Jeon, S. J.; Cho, B. R. *Chem. Phys. Lett.* **2005**, *410*, 312.
(39) Bozio, R.; Cecchetto, E.; Fabbrini, G.; Ferrante, C.; Maggini, M.; Menna, E.; Pedron, D.; Ricco, R.; Signorini, R.; Zerbetto, M. *J. Phys. Chem. A* **2006**, *11*, 6459.
(40) Huang, F.; Tian, Y. Q.; Chen, C. Y. *J. Phys. Chem. C* **2007**, *111*, 10673.
(41) Chang, C. J.; Nolan, E. M.; Jaworski, J.; Okamoto, K. I.; Hayashi, Y.; Sheng, M.; Lippard, S. J. *Inorg. Chem.* **2004**, *43*, 6774.
(42) Chen, X.-Y.; Shi, J.; Li, Y.-M.; Wang, F. L.; Wu, X.; Guo, Q. X.; Liu, L. *Org. Lett.* **2009**, *11*, 4426.
(43) Meng, X. M.; Wang, S. X.; Li, Y. M.; Zhu, M. Z.; Guo, Q. X. *Chem. Commun.* **2012**, *48*, 4196.
(44) Masanta, G.; Lim, C. S.; Kim, H. J.; Han, J. H.; Kim, H. M.; Cho, B. R. *J. Am. Chem. Soc.* **2011**, *133*, 5698.
(45) Divya, K. P.; Sreejith, S.; Balakrishna, B.; Jayamurthy, P.; Anees, P.; Ajayaghosh, A. *Chem. Commun.* **2010**, *46*, 6069.
(46) Zhao, C. C.; Zhang, Y. L.; Feng, P.; Cao, J. *Dalton Trans.* **2012**, *41*, 831.
(47) Li, Y.; Shi, L.; Qin, L. X.; Qu, L. L.; Jing, C.; Lan, M.; Jamesb, T. D.; Long, Y. T. *Chem. Commun.* **2011**, *47*, 4361.
(48) Mukherjee, T.; Pessoa, J. C.; Kumar, A.; Sarkar, A. R. *Dalton Trans.* **2012**, *41*, 5260.
(49) Becke, A. D. *J. Chem. Phys.* **1993**, *98*, 5648.
(50) Lee, C.; Yang, W.; Parr, R. G. *Phys. Rev. B* **1988**, *37*, 785.
(51) Becke, A. D. *J. Chem. Phys.* **1996**, *104*, 1040.
(52) Yanai, T.; Tew, D. P.; Handy, N. C. *Chem. Phys. Lett.* **2004**, *393*, 51.
(53) Jacquemin, D.; Perpete, E. A.; Scalmani, G.; Frisch, M. J.; Kobayashi, R.; Adamo, C. *J. Chem. Phys.* **2007**, *126*, 144105.
(54) Zhao, Y.; Truhlar, D. G. *J. Chem. Theory Comput.* **2005**, *1*, 415.
(55) Zhao, Y.; Truhlar, D. G. *J. Phys. Chem. A* **2004**, *108*, 6908.
(56) Zhao, Y.; Truhlar, D. G. *Theor. Chem. Acc.* **2008**, *120*, 215.
(57) Cramer, C. J.; Truhlar, D. G. *Phys. Chem. Chem. Phys.* **2009**, *11*, 10757.
(58) Hehre, W. J.; Ditchfield, R.; Pople, J. A. *J. Chem. Phys.* **1972**, *56*, 2257.
(59) Francl, M. M.; Pietro, W. J.; Hehre, W. J.; Binkley, J. S.; Gordon, M. S.; DeFrees, D. J.; Pople, J. A. *J. Chem. Phys.* **1982**, *77*, 3654.
(60) Frisch, M. J.; Trucks, G. W.; Schlegel, H. B.; Scuseria, G. E.; Robb, M. A.; Cheeseman, J. R.; Scalmani, G.; Barone, V.; Mennucci, B.; Petersson, G. A.; Nakatsuji, H.; Caricato, M.; Li, X.; Hratchian, H. P.; Izmaylov, A. F.; Bloino, J.; Zheng, G.; Sonnenberg, J. L.; Hada, M.; Ehara, M.; Toyota, K.; Fukuda, R.; Hasegawa, J.; Ishida, M.; Nakajima, T.; Honda, Y.; Kitao, O.; Nakai, H.; Vreven, T.; Montgomery, J. A., Jr.; Peralta, J. E.; Ogliaro, F.; Bearpark, M.; Heyd, J. J.; Brothers, E.; Kudin, K. N.; Staroverov, V. N.; Kobayashi, R. Normand, J.; Raghavachari, K.; Rendell, A.; Burant, J. C.; Iyengar, S. S.; Tomasi, J.; Cossi, M.; Rega, N.; Millam, J. M.; Klene, M.; Knox, J. E.; Cross, J. B.; Bakken, V.; Adamo, C.; Jaramillo, J.; Gomperts, R.; Stratmann, R. E.; Yazyev, O.; Austin, A. J.; Cammi, R.; Pomelli, C.; Ochterski, J. W.; Martin, R. L.; Morokuma, K.; Zakrzewski, V. G.; Voth, G. A.; Salvador, P.; Dannenberg, J. J.; Dapprich, S.; Daniels, A. D.; Farkas, O.; Foresman, J. B.; Ortiz, J. V.; Cioslowski, J. Fox, D. J. *Gaussian 09*, revisions A.02 and B.01; Gaussian, Inc.: Wallingford, CT, 2009.
(61) Cheshmedzhieva, D.; Ivanova, P.; Stoyanov, S.; Tasheva, D.; Dimitrova, M.; Ivanov, I.; Ilieva, S. *Phys. Chem. Chem. Phys.* **2011**, *13*, 18530.
(62) Leng, W. N.; Bazan, G. C.; Kelley, A. M. *J. Chem. Phys.* **2009**, *130*, 044501.
(63) Kogej, T.; Beljonne, D.; Meyers, F.; Perry, J. W.; Marder, S. R.; Brédas, J. L. *Chem. Phys. Lett.* **1998**, *298*, 1.
(64) Orr, B. J.; Ward, J. F. *Mol. Phys.* **1971**, *20*, 513.
(65) Bishop, D. M.; Luis, J. M.; Kirtman, B. *J. Chem. Phys.* **2002**, *116*, 9729.
(66) Beljonne, D.; Wenseleers, W.; Zojer, E.; Shuai, Z. G.; Vogel, H.; Pond, S. J. K.; Perry, J. W.; Marder, S. R.; Brédas, J. L. *Adv. Funct. Mater.* **2002**, *12*, 631.
(67) Anderson, W. P.; Edwards, W. D.; Zerner, M. C. *Inorg. Chem.* **1986**, *25*, 2728.
(68) Huang, S.; Ren, A. M.; Zou, L. Y.; Zhao, Y.; Guo, J. F.; Feng, J. K. *Dyes Pigments* **2011**, *91*, 248.
(69) Zhao, Y.; Ren, A. M.; Zou, L. Y.; Guo, J. F.; Feng, J. K. *Theor. Chem. Acc.* **2011**, *130*, 61.
(70) Zhang, C.; Dalton, L. R.; Oh, M. C.; Zhang, H.; Steier, W. H. *Chem. Mater.* **2001**, *13*, 3043.
(71) Cho, B. R.; Son, K. H.; Lee, S. H.; Song, Y. S.; Lee, Y. K.; Jeon, S. J.; Choi, J. H.; Lee, H.; Cho, M. *J. Am. Chem. Soc.* **2001**, *123*, 10039.
(72) Chung, S. J.; Rumi, M.; Alain, V.; Barlow, S.; Perry, J. W.; Marder, S. R. *J. Am. Chem. Soc.* **2005**, *127*, 10844.
(73) Pond, S. J. K.; Tsutsumi, O.; Rumi, M.; Kwon, O.; Zojer, E.; Brédas, J. L.; Marder, S. R.; Perry, J. W. *J. Am. Chem. Soc.* **2004**, *126*, 9291.
(74) Cai, Y. B.; Zhan, J. H.; Hai, Y.; Zhang, J. L. *Chem.—Eur. J.* **2012**, *18*, 4242.
(75) Cramer, C. J. *Essentials of Computational Chemistry: Theories and Models*; Wiley: New York, 2002; p 87.
(76) Kim, K. S.; Tarakeshwar, P.; Lee, J. Y. *Chem. Rev.* **2000**, *100*, 4145.
(77) Boys, S. F.; Bernardi, F. *Mol. Phys.* **1970**, *19*, 553.
(78) Zheng, X. Y.; Wang, X. Y.; Yi, S. F.; Wang, N. Q.; Peng, Y. M. *J. Comput. Chem.* **2010**, *31*, 1458.
(79) Vainrub, A.; Pettitt, B. M. *Biopolymers* **2003**, *68*, 265.
(80) Yang, R.; Guo, X. F.; Wang, W.; Zhang, Y.; Jia, L. H. *J. Fluoresc.* **2012**, *22*, 1065.
(81) Wu, J. S.; Liu, W. M.; Ge, J. C.; Zhang, H. Y.; Wang, P. F. *Chem. Soc. Rev.* **2011**, *40*, 3483.
(82) Weissleder, R.; Ntziachristos, V. *Nat. Med.* **2003**, *9*, 123.
(83) Liu, X. T.; Guo, J. F.; Ren, A. M.; Huang, S.; Feng, J. K. *J. Org. Chem.* **2012**, *77*, 585.
(84) Sumalekshmy, S.; Fahrni, C. J. *Chem. Mater.* **2011**, *23*, 483.